Discovery of a Potent Small-Molecule Antagonist of Inhibitor of Apoptosis (IAP) Proteins and Clinical Candidate for the Treatment of Cancer (GDC-0152)

John A. Flygare,*,[†] Maureen Beresini,[‡] Nageshwar Budha,[§] Helen Chan,[∥] Iris T. Chan,[⊥] Sravanthi Cheeti,[§] Frederick Cohen,[†] Kurt Deshayes,[#] Karl Doerner,[○] S. Gail Eckhardt,[◆] Linda O. Elliott,[‡] Bainian Feng,[†] Matthew C. Franklin,[#] Stacy Frankovitz Reisner,[‡] Lewis Gazzard,[†] Jason Halladay,[∥] Sarah G. Hymowitz,[¶] Hank La,[∥] Patricia LoRusso,[◇] Brigitte Maurer,[¶] Lesley Murray,[○] Emile Plise,[∥] Clifford Quan,[#] Jean-Philippe Stephan,[‡] Shin G. Young,[∥] Jeffrey Tom,[#] Vickie Tsui,[†] Joanne Um,[†] Eugene Varfolomeev,[#] Domagoj Vucic,[#] Andrew J. Wagner,[○] Heidi J. A. Wallweber,[¶] Lan Wang,[†] Joseph Ware,[§] Zhaoyang Wen,[†] Harvey Wong,[∥] Jonathan M. Wong,[†] Melisa Wong,[†] Susan Wong,[∥] Ron Yu,[▽] Kerry Zobel,[#] and Wayne J. Fairbrother*,[#]
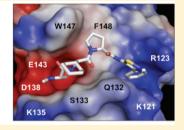
Departments of [†]Discovery Chemistry, [‡]Biochemical and Cellular Pharmacology, [§]Clinical Pharmacology, [∥]Drug Metabolism and Pharmacokinetics, [⊥]Oncology Exploratory Clinical Development, [#]Early Discovery Biochemistry, [○]Translational Oncology, [¶]Structural Biology, and [▽]Biostatistics, Genentech, Inc., 1 DNA Way, South San Francisco, California 94080, United States

[◆]Division of Medical Oncology, University of Colorado Denver Anschutz Medical Campus, Aurora, Colorado 80045, United States

[◇]Department of Oncology, Barbara Ann Karmanos Cancer Institute, Wayne State University, Detroit, Michigan 48201, United States

[○]Center for Sarcoma and Bone Oncology, Dana Farber Cancer Institute, 44 Binney Street, Boston, Massachusetts 02115, United States

Ⓢ *Supporting Information*

ABSTRACT: A series of compounds were designed and synthesized as antagonists of cIAP1/2, ML-IAP, and XIAP based on the N-terminus, AVPI, of mature Smac. Compound **1** (GDC-0152) has the best profile of these compounds; it binds to the XIAP BIR3 domain, the BIR domain of ML-IAP, and the BIR3 domains of cIAP1 and cIAP2 with K_i values of 28, 14, 17, and 43 nM, respectively. These compounds promote degradation of cIAP1, induce activation of caspase-3/7, and lead to decreased viability of breast cancer cells without affecting normal mammary epithelial cells. Compound **1** inhibits tumor growth when dosed orally in the MDA-MB-231 breast cancer xenograft model. Compound **1** was advanced to human clinical trials, and it exhibited linear pharmacokinetics over the dose range (0.049 to 1.48 mg/kg) tested. Mean plasma clearance in humans was 9 ± 3 mL/min/kg, and the volume of distribution was 0.6 ± 0.2 L/kg.

K(ML-IAP-BIR) = 0.014 μM
K(XIAP-BIR3) = 0.028 μM
K(XIAP-BIR2) = 0.112 μM
K(cIAP1-BIR3) = 0.017 μM
K(cIAP2-BIR3) = 0.043 μM

INTRODUCTION

Apoptosis is a physiological cell-death program that is critical for the maintenance of tissue homeostasis. This process results in the removal of unwanted cells such as those with potentially harmful genomic mutations or alterations in cell-cycle control. Cancer cells, unlike normal cells, are under stress and highly dependent on aberrations in the apoptosis signaling pathways to remain viable. Therefore, drugs that can restore apoptosis in tumor cells might be effective for the treatment of cancer.

Members of the mammalian inhibitor of apoptosis (IAP) family of proteins, including X chromosome-linked IAP (XIAP), cellular IAP 1 (cIAP1), cellular IAP 2 (cIAP2), and melanoma IAP (ML-IAP), are frequently overexpressed in cancer cells,[1−5] where they confer protection against a variety of pro-apoptotic stimuli.[6−13] The IAP proteins have also been demonstrated to function in the regulation of signal transduction pathways associated with malignancy.[14−25] In particular, the cIAP proteins regulate TNFα-mediated NF-κB activation via their C-terminal RING ubiquitin E3-ligase domains, which have been shown to ubiquitinate receptor interacting protein (RIP)-1 and NF-κB inducing kinase, NIK.[26]

Efforts to target the IAP proteins have focused on the design of small molecules that mimic the binding of the endogenous IAP antagonist second mitochondria-derived activator of caspases/direct IAP-binding protein with low pI (Smac/DIABLO)[27,28] to a shallow groove on the surface of select IAP baculoviral IAP repeat (BIR) domains.[29] The IAP BIR domains are approximately

80-amino acid zinc-binding domains that are necessary for the antiapoptotic function of the IAP proteins. The third BIR domain (BIR3) of XIAP is a specific inhibitor of caspase-9,[30−33] while the BIR2 domain is necessary for potent inhibition of caspases-3 and -7.[34−38] Antagonism of XIAP-mediated inhibition of these caspases is required for efficient caspase-dependent cell death via both the extrinsic death receptor-mediated and the intrinsic mitochondrial-mediated apoptosis pathways.[39]

The four amino-acid N-terminus of mature Smac (AVPI) is capable of antagonizing XIAP with a binding affinity of approximately 500 nM against the BIR3 domain.[40] AVPI also binds with high affinity to the BIR3 domains of cIAP1/2, the single BIR domain of ML-IAP, and with lower affinity to the BIR2 domain of XIAP. In an effort to uncover lead matter capable of mimicking these interactions, we undertook several large high-throughput-screening campaigns. Screening greater than two million compounds for binding to the ML-IAP BIR domain failed to uncover any viable starting points; thus, we relied solely on a peptidomimetic approach. Herein, we report the design, synthesis, and evaluation of a series of Smac mimetics that were based on the AVPI tetrapeptide. This peptide sequence has served as the lead structure for several reports detailing the evaluation of monovalent and bivalent small-molecule Smac mimetics capable of antagonizing the IAP proteins.[41−46] We sought to evolve the peptide into a compound with improved potency, pharmacokinetic properties, and cell-killing characteristics that would allow us to evaluate the effectiveness of IAP antagonism in human clinical trials. We took a systematic approach to evaluate the contributions of each substituent in the P1 through P4 positions using a combination of structure-based design and targeted compound library generation. The efforts culminated in the discovery of compound **1** (GDC-0152), a potent antagonist of cIAP1/2, ML-IAP, and XIAP and the first compound targeting this class of proteins to enter clinic trials.

■ SYNTHESIS

Compounds were prepared using either a solid-phase (Scheme 1) or a solution-phase synthesis (Schemes 2 and 3). In the solid-phase method, DFPE polystyrene resin was treated with 2, 2-diphenethylamine, and sodium cyanoborohydride to provide amine **2**. Substituted proline (R_1) and valine (R_2) derivatives were prepared using HATU/DIPEA and HBTU/HOBt, DIPEA, respectively, to yield **3** and **4**. N-Capped anilines (**6** or **7**) were made using two procedures from intermediate **4**. In the first method, Fmoc-alanine was coupled to **4** followed by a reductive amination with an aldehyde and sodium cyanoborohydride to give enantiomerically pure compound **6**. Alternatively, using the peptoid synthesis method developed by Zuckermann,[47] **4** was coupled with bromopropionoic acid followed by displacement with a primary amine to yield racemic compound **7**. The solution synthesis of P4 derivatives (Scheme 2) all utilized carboxylic acid **8**. Primary amines with a saturated or unsaturated two-carbon spacer and an aromatic ring (**9**) were coupled to the carboxylic acid using EDC/HOBt to yield **10**. The synthesis of **1** is outlined in Scheme 3. Thiadiazole **11** was coupled to Boc-proline using EDC/HOBt to yield **12**. Boc-cyclohexylglycine and Boc-methylalanine were sequentially coupled to **13** using BOP, which, after deprotection with hydrochloric acid, yielded **1**.

Scheme 1. Solid Phase Synthesis of P1, P2, and P3 Derivatives[a]

[a]Reagents and conditions: (a) 2,2-diphenethylamine, NaCNBH$_3$; 1% AcOH/DMF. (b) FmocPro, HATU; DIPEA/DMF (X = −CH$_2$−). (c) Fmoc-Val(R$_2$ = isopropyl), HBTU/HOBt, DIPEA/DMF. (d) FmocAla, HBTU/HOBt, DIPEA/DMF. (e) Aldehyde, NaCNBH$_3$; 1% AcOH/DMF. (f) TFA/H$_2$O. (g) Bromopropionoic acid, DIC/DMF. (h) Primary amine, DMF. (i) TFA/H$_2$O.

Scheme 2. Synthesis of P4 Derivatives[a]

[a]Reagents and conditions: (a) DIC, HOBt, CH$_2$Cl$_2$, 24 h. (b) TFA, CH$_2$Cl$_2$.

Scheme 3[a]

[a]Reagents and conditions: (a) EDC, HOBt, DIPEA, DMF, 24 h; (b) HCl, dioxane; (c) TEA, CH$_2$Cl$_2$; (d) Boc-Chg, BOP, DIPEA, DMF, 3 h; (e) HCl, dioxane; (f) TEA, CH$_2$Cl$_2$; (g) Boc-MeAla, BOP, DIPEA, DMF, 3 h; (h) HCl, dioxane.

■ RESULTS AND DISCUSSION

We used an analysis of our previously published 2.3-Å resolution crystal structure of Ala-Val-Pro-2,2-diphenethylamine

Table 1. Structure and Potency of IAP Antagonists[a]

Compound	R$_1$	X	R$_2$	R$_3$	K_i (μM)[b] XIAP-BIR3	K_i (μM)[b] MLXBIR3SG
6a	diphenethylamine (NH)	CH$_2$	isopropyl	CH$_3$	0.43[c]	0.03[c]
6b	diphenethylamine (NH)	S	cyclohexyl	CH$_3$	0.19[c]	0.03[c]
6c	diphenethylamine (NH)	CH$_2$	isopropyl	cyclopropylmethyl	7.6 ± 0.5	0.46 ± 0.12
6d	diphenethylamine (NH)	CH$_2$	isopropyl	2,3-dihydroxypropyl (HO OH)	0.8 ± 0.2	0.08 ± 0.02
10a	diphenethylamine (NH)	CH$_2$	cyclohexyl	CH$_3$	0.41 ± 0.11	0.07 ± 0.01
10b	4-chlorobenzylamine (H N)	CH$_2$	cyclohexyl	CH$_3$	0.7 ± 0.2	0.09 ± 0.02
14	thiadiazolyl-phenyl (NH)	CH$_2$	phenyl	CH$_3$	0.035 ± 0.003	0.016 ± 0.003
1	thiadiazolyl-phenyl (NH)	CH$_2$	cyclohexyl	CH$_3$	0.028 ± 0.011	0.014 ± 0.006

[a]K_i determined as described in ref [50]. [b]Average of two measurements. [c]Single measurement

bound to the BIR domain of ML-IAP[48] as our starting point for the design of our compounds. From this structure, we understood that the alanine methyl group in P1 would be difficult to replace as the methyl group was buried within a hydrophobic pocket formed by the side chains of Leu131, Trp134, and Glu143. Additional evidence for the need to maintain this methyl group came from the phage-display of naive peptide libraries.[49] In that work Ala was the only residue observed at the N-terminus following three sorts of phage libraries of linear peptides against both ML-IAP-BIR and XIAP-BIR3. The other three positions (P2−P4) all tolerated some level of substitution. The N-terminus of the peptide binds in an acidic site on the BIR domains, with the amino group of Ala interacting with the side-chain carboxylates of Asp138 and Glu143 in ML-IAP, Glu314 in XIAP, and Asp320 and Glu325 in cIAP1. Several bond vectors from this nitrogen could be extended to potentially pick up additional binding interactions with the BIR domains. To explore these interactions, libraries of nitrogen-capped derivatives were made, fixing diphenethyl-amine in P4, proline in P3, and valine in P2 as detailed in Scheme 1. Primary amines and aldehydes were selected for this library by carefully choosing derivatives from randomly generated diversity sets of these compounds that contained functionality that could potentially interact with the BIR domain. Several hundred compounds were made and individually purified by reverse-phase HPLC prior to analysis. The compounds derived from the primary amines (7) were assayed as diastereomeric mixtures, and the compounds from the aldehydes (6) were enantiomerically pure. The binding affinities of these compounds for ML-IAP-BIR and XIAP-BIR3 were

determined using a fluorescence polarization-based competition assay. No substituent in this position was more effective than a methyl group. For example, as shown in Table 1, replacement of the P1 methyl group with either a cyclopropylmethyl group (6c) or a 2, 3-dihydroxypropyl group (6d) failed to achieve the same level of binding affinity versus either protein.

For the analysis of the P2 position, we fixed methyl-Ala in P1 and proline in P3 utilizing the solid phase synthesis in Scheme 1. The P2 position tolerated the most substitution in our prior peptide-phage selection; thus, we anticipated that this area would accommodate a wide range of functionality. The endogenous valine makes van der Waals contact with the β-methylene of Ser133 in ML-IAP, but compared with the other side chains in the sequence, this contribution is minimal. Consistent with this observation, very little difference was noted in binding affinity when the valine was replaced with a large hydrophobic substituent such as a cyclohexyl (10a) or t-butyl (data not shown) group. The rotation of bulky P2 side chains is restricted by the presence of a Pro at P3, and these interactions favor a peptide conformation that optimizes the interactions between P2-Pro and the BIR domains. Larger P2 side chains also improve the proteolytic stability of the P2-Pro peptide bond (data not shown).

The proline in P3 productively orients the P1 and P4 substituents. We have published previous efforts to modify this region with a 7−5 bicyclic ring,[50] an azabicyclooctane fuzed ring,[48] or a thiazoline.[51] Substitution directly off the proline ring allows for favorable interactions with Phe148 of ML-IAP or Phe330 of cIAP1-BIR3 but can result in a steric clash with the corresponding Tyr324 of XIAP-BIR3. We have exploited this

difference to make compounds that have selectivity (>2,000-fold) for cIAP1 over XIAP.[52] Given our desire in this work to create a pan-specific compound, we limited our exploration of proline replacements to changes directly in the ring. As illustrated in Table 1, substitution of a methylene with a sulfur is tolerated without any loss of binding affinity (**6b**).
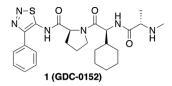
Having used a solid-phase method to rapidly scan P1−P3, we turned to the solution-phase synthesis outlined in Scheme 2 to assess the binding contributions of the P4 residue. MeAla, ChGly, and Pro were fixed in the P1, P2, and P3 positions, respectively, and primary amines were added to the terminal carboxylic acid. The peptide-phage data revealed a preference for an aromatic ring in the P4 position over the endogenous isoleucine of Smac. Consistent with this, the crystal structure of Ala-Val-Pro-2,2-diphenethylamine bound to the BIR domain of ML-IAP showed one of the phenyl rings occupying a hydrophobic pocket defined by Thr116, Gly130, Gln132, and the aliphatic portions of Lys121 and Arg123. With this structural information, we limited our initial exploration to primary amines with a one- or two-carbon spacer connected to an aromatic ring. Compounds were selected based on their ability to add additional binding interactions in this well-defined pocket. Of particular interest were the thiadiazole compounds **1** and **14**, both of which showed improved binding affinity relative to diphenethylamine. We initiated further studies with compound **1**.
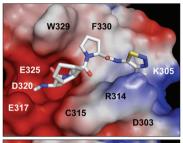
To understand the specific interactions resulting in high-affinity interactions, crystal structures were determined of **1** bound to XIAP chimeras of ML-IAP BIR (MLXBIR3SG) and cIAP1 BIR3 (cXBIR3CS) domains (Figure 1). Key interactions are consistent between the two structures including the critical hydrogen-bond interaction with Asp138 in ML-IAP and the corresponding Asp320 in cIAP1. This helps position the α-methyl group of the methyl-Ala in the P1 cavity formed in both complexes. In both examples, the thiadiazole heterocycle positions the attached aromatic ring optimally within the hydrophobic P4 pocket.

As we desired a pan-selective antagonist, we evaluated the thiadiazole (**1**) for its ability to bind to the BIR domain of ML-IAP and the BIR2 and BIR3 domains of cIAP1, cIAP2, and XIAP using a fluorescence polarization-based competition assay (Figure 2 and Table 2). The ML-IAP/XIAP chimeric BIR domain MLXBIR3SG, which retains the native ML-IAP-BIR Smac-peptide-binding site,[53] was used as a surrogate for the ML-IAP BIR domain. Compound **1** binds to XIAP-BIR3, cIAP1-BIR3, cIAP2-BIR3, and the single BIR domain of ML-IAP with affinities in the low nanomolar range ($K_i < 50$ nM). By contrast, the K_i values of **1** for cIAP1-BIR2 and cIAP2-BIR2 are approximately 10 μM.

The ability of **1** to block protein−protein interactions that involve IAP proteins and pro-apoptotic molecules was evaluated by immunoprecipitation and immunoblotting. Using transiently transfected HEK293T cells, **1** was shown to disrupt XIAP binding to partially processed caspase-9 (Figure 3A) and to disrupt the association of ML-IAP, cIAP1, and cIAP2 with Smac (Figure 3B). In melanoma SK-MEL28 cells, the endogenous association of ML-IAP and Smac was effectively also abolished by **1** (Supporting Information).

To assess how these interactions with IAP proteins translated into cell killing, compound **1** was tested in a three-day cell viability assay. As shown in Figure 4A, **1** led to a decrease in cell viability in the MDA-MB-231 breast cancer cell line while having no effect on normal human mammary epithelial
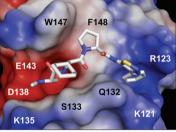

1 (GDC-0152)

Figure 1. Solvent-accessible surface representation of the peptide-binding site of (upper panel) the 1.79-Å resolution crystal structure of the cIAP1/XIAP chimeric BIR3 domain (cXBIR3CS) (PDB ID 3UW4) and (lower panel) the 1.71-Å resolution crystal structure of the ML-IAP/XIAP chimeric BIR domain (MLXBIR3SG) (PDB ID 3UW5) in complex with **1**. The protein surfaces are color-coded according to the electrostatic surface potentials: red is negatively charged; blue is positively charged. This figure was produced using the program PyMol (www.pymol.org).
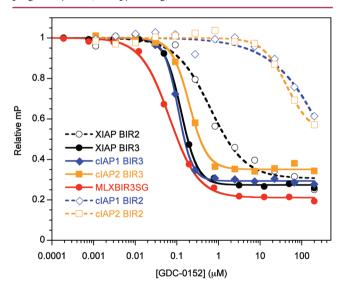

Figure 2. Competitive binding curves for **1** binding to MLXBIR3SG and select BIR domains of XIAP, cIAP1, and cIAP2. The K_i values (Table 1) were calculated from IC_{50} values as described previously.[63]

cells (HMEC). This result was consistent with the moderate cell permeability of **1** in MDCK cells (A and B; $P_{app} = 1.8 \times 10^{-6}$ cm/s).

The effect of **1** on the activity of the effector caspases 3 and 7 in the MDA-MB-231 breast cancer cell line was measured to determine the specific mechanism of action. Compound **1** was

Table 2. Summary of K_i Values (μM) for Compound 1

IAP protein BIR domain	K_i(1)
MLXBIR3SG	0.014 ± 0.006^a
XIAP-BIR3	0.028 ± 0.011^b
XIAP-BIR2	0.112^c
cIAP1-BIR3	0.017^c
cIAP1-BIR2	14.5^c
cIAP2-BIR3	0.043^c
cIAP2-BIR2	9.6^c

[a] Average of 5 measurements. [b] Average of 4 measurements. [c] These values were taken from Figure 2.
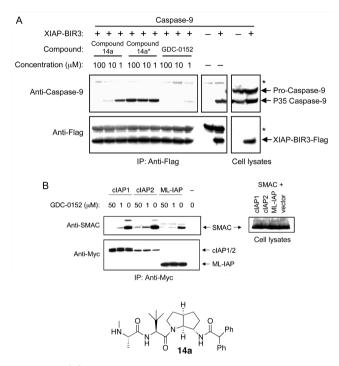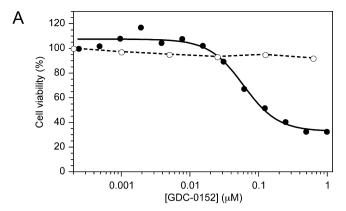

Figure 3. (A) HEK293T cells were transiently transfected with caspase-9 and Flag-tagged XIAP-BIR3 domain or empty vector. Cells were lysed, and lysates were incubated with the previously published IAP protein antagonist compound 14a,[48] its non-IAP protein binding stereoisomer, compound 14a* (a negative control),[48] or 1. Immunoprecipitation was performed with anti-Flag antibody, and samples were immunoblotted with anticaspase-9 and anti-Flag antibodies. Whole-cell lysates are shown in the right panels. Astericks denote nonspecific bands from immunoprecipitations. (B) HEK293T cells were transiently transfected with Smac and Myc-tagged cIAP1, cIAP2, ML-IAP, or empty vector. Cells were lysed, and lysates were incubated with the indicated concentrations of 1 and immunoprecipitated with anti-Myc antibody (left panels). Samples were then immunoblotted with anti-Smac and anti-Myc antibodies. Whole-cell lysates are shown in the right panel.

found to activate caspases 3 and 7 in a dose- and time-dependent manner as shown in Figure 4B. To probe the specificity of the observed effects, the enantiomer of 1 was assessed at the 24-h time point and found to not activate the caspases at concentrations up to ~10 μM. The potency of the caspase activation correlated well with the cell viability results and provided strong evidence that the cell killing was mediated through the desired apoptosis signaling culminating in caspase-3/7 activation.
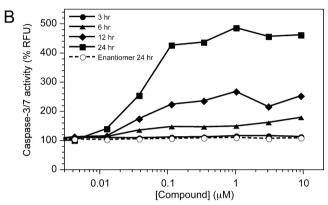

Figure 4. (A) MDA-MB-231 breast carcinoma cells (solid symbols) and HMECs (open symbols) were treated with the indicated concentrations of 1. Cell death was assessed using the CellTiter-Glo luminescent cell viability assay 72 h following the start of treatment. (B) Effect of 1 (solid symbols) or its enantiomer (open symbols) on caspase-3 and -7 activities in MDA-MB-231 cells assessed using the Apo-ONE homogeneous caspase-3/7 assay.

Previous studies have demonstrated that Smac mimetics can induce autoubiquitination activity and rapid proteasomal degradation of cIAP1.[54] Consistent with these studies, 1 was shown to induce rapid degradation of cIAP1 in A2058 melanoma cells (Figure 5). Compound 1 effectively induces
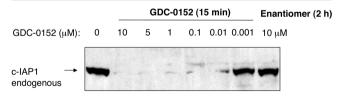

Figure 5. A2058 cells were treated with increasing amounts of 1 or with 10 μM of its enantiomer for the indicated time periods. Cells were lysed, and lysates were immunoblotted with anti-c-IAP1 and antibody.

degradation of cIAP1 at concentrations as low as 10 nM, consistent with its affinity for cIAP1, while its enantiomer, which does not bind to cIAP1, has no effect following a 2-h exposure at a concentration of 10 μM.

Pharmacokinetic optimization was performed in parallel with the optimization of potency. We focused on the identification of compounds that would enable both preclinical proof of concept in an *in vivo* efficacy model and testing of IAP antagonism in the clinic. The compounds were not dissolution limited as all had favorable solubility properties. The kinetic
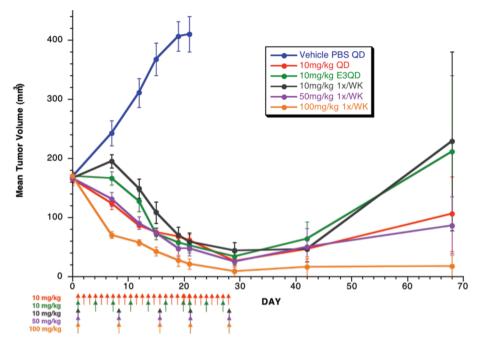
Figure 6. Efficacy of **1** compared to vehicle control in human-tumor xenograft mouse models of MDA-MB-231 breast cancer. Compounds were dosed as an oral solution at the indicated time intervals and doses. Compound **1** showed significant dose-dependent growth inhibition throughout dosing (*p*-value < 0.001 for all doses).

solubility of compound **1** was 40 mg/mL at pH 5.5, 2.0 mg/mL at pH 6.7, and 0.46 mg/mL at pH 7.7. Compound **1** had moderate predicted hepatic clearance based on metabolic stability assays conducted using human liver microsomes (data not shown). Additional *in vitro* ADME evaluation also included an assessment of plasma−protein binding and blood−plasma partitioning. The plasma−protein binding of **1** was evaluated in mouse, rat, rabbit, dog, monkey, and human plasma by equilibrium dialysis using [^{14}C]**1**. Plasma−protein binding of **1** was moderate and comparable among mice (88−91%), rats (89−91%), dogs (81−90%), monkeys (76−85%), and humans (75−83%) over the range of concentrations investigated (0.1−100 μM); higher plasma−protein binding was observed in rabbits (95−96%). Compound **1** did not preferentially distribute to red blood cells with blood−plasma partition ratios ranging from 0.6 to 1.1 in all species tested.

The *in vivo* pharmacokinetics for **1** were evaluated initially in mice in order to enable efficacy studies in human-tumor mouse xenograft models. The monotrifluoroacetic acid salt of **1** was dosed orally in female mice at 100 mg/kg as a solution in phosphate-buffered saline (PBS). Significant exposure was achieved with a C_{max} of 53.7 μM and AUC of 203.5 h·μM. The *in vivo* efficacy studies of **1** were performed using human-tumor xenograft mouse models of MDA-MB-231 breast cancer with a variety of dosing schedules and regimens. These *in vivo* studies demonstrated that **1** has robust antitumor activity as a single agent as shown in Figure 6. Dosing once weekly with 10, 50, or 100 mg/kg resulted in significant tumor volume reduction (*p*-value < 0.001 for all doses). Similar results were obtained when dosed at 10 mg/kg daily or every third day for three weeks. The initial rate of regression was greatest with doses of 100 mg/kg given once a week, although by day 21 all groups dosed with **1** had experienced between 85 and 95% inhibition of tumor growth, with four to six complete responses, relative to the vehicle-control group. In mice that experienced less than a partial response (defined as >50% but <100% reduction in tumor volume, compared with the starting tumor volume), tumors resumed growth after the final doses of **1** were administered. Notably, **1** was well tolerated by all groups, and by day 28, all remaining mice had a mean gain in body weight of ≥5%. A transient loss in body weight was observed for mice that were given weekly doses of 100 mg/kg, although body weights were similar among all groups on day 28.

The preclinical pharmacokinetics of **1** were investigated in mouse, rat, dog, and monkeys following single-dose intravenous (IV) administration. Following a low IV dose (1 mg/kg), **1** had a high plasma clearance (>80% of hepatic blood flow) in nude mice, Sprague−Dawley rats, and cynomolgus monkeys, and a moderate plasma clearance (52% of hepatic blood flow) in beagle dogs (Table 3). At high doses (100 mg/kg in mice; 20 mg/kg in rats, dogs, and monkeys), mechanisms of clearance from plasma became saturated in mouse and rat but not in the monkey and dog.
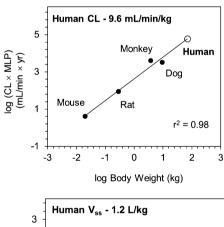
Human clearance was predicted using *in vivo* preclinical pharmacokinetic data and allometry adjusted for maximum life potential (Figure 7) or using *in vitro−in vivo* extrapolation of hepatocyte stability data. Both methods resulted in similar moderate human clearance predictions of 9.6 (allometry) and 10 mL/min/kg (*in vitro−in vivo* extrapolation). Human volume of distribution was predicted to be moderate at 1.2 L/kg using allometry (Figure 7).

On the basis of the human PK predictions, the antitumor efficacy, and the favorable safety profile observed in preclinical species, compound **1** was advanced for evaluation in humans. In humans, **1** exhibited linear pharmacokinetics over the dose range (0.049 to 1.48 mg/kg) tested (Figure 8). Mean plasma clearance was 9 ± 3 mL/min/kg and volume of distribution was 0.6 ± 0.2 L/kg (Supporting Information, Table S2), in good agreement with preclinical predictions.

Table 3. Pharmacokinetics Parameters (mean ± SD) of 1 in Mouse, Rat, Dog, and Monkey after IV Bolus Administration[a]

parameter	nude mouse	Sprague–Dawley rat	beagle dog	cynomolgus monkey
sex	female	male	male	male
N	27	3	3	3
low dose (mg/kg)	1	1	1	1
CL (mL/min/kg)	72	67 ± 10	16 ± 3	47 ± 4
V_{ss} (L/kg)	1.6	2.0 ± 0.3	1.0 ± 0.2	1.60 ± 0.04
$t_{1/2}$ (h)	0.4	0.43 ± 0.05	0.9 ± 0.1	0.44 ± 0.05
C_{max} (μM)	1.4	1.1 ± 0.2	3.8 ± 0.1	1.46 ± 0.04
$AUC_{0-\infty}$ (h·μM)	0.5	0.51 ± 0.08	2.1 ± 0.4	0.71 ± 0.06
sex	female	male	male/ female	male
N	27	3	2	3
high dose (mg/kg)	100	20	20	20
CL (mL/min/kg)	23	27 ± 2	19	36 ± 6
V_{ss} (L/kg)	1.7	1.7 ± 0.2	1.5	2.2 ± 0.3
$t_{1/2}$ (h)	2.9	0.84 ± 0.06	2.0	0.77 ± 0.01
C_{max} (μM)	118.6	31 ± 4	30	24 ± 3
$AUC_{0-\infty}$ (h·μM)	147	25 ± 2	36	19 ± 3

[a]$AUC_{0-\infty}$ = area under the concentration–time curve from time zero to infinity; CL = total plasma clearance; C_{max} = highest observed plasma concentration of 1; $t_{1/2}$ = terminal half-life; V_{ss} = volume of distribution at steady state. Compound 1 hydrochloride salt in 10% hydroxypropyl-β-cyclodextrin was used in the mouse studies; 1-TFA salt in phosphate-buffered saline was used in the rat, monkey, and dog studies.
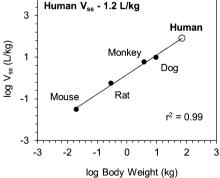

Figure 7. Prediction of human clearance and volume of distribution of compound 1 using allometric methods for clearance (CL) and volume of distribution (V_{ss}).

CONCLUSIONS

Using a combination of structure-based design and solid-phase library synthesis, we have made a series of compounds that

mimic the four-amino acid N-terminus of mature Smac. From these studies, 1 was found to be a potent antagonist of cIAP1, cIAP2, ML-IAP, and XIAP with the ability to disrupt IAP binding to pro-apoptotic proteins such as partially processed caspase-9 and Smac. X-ray crystallographic analysis confirmed that 1 binds to the Smac-binding site of the cIAP1 BIR3 and ML-IAP BIR domains with a binding mode very similar to that observed for Smac-derived peptides. As described previously for Smac mimetics, 1 also induces autoubiquitination activity and rapid proteasomal degradation of cIAP1. Cell-based assays confirmed that 1 promoted the activation of caspase-3 and -7, resulting in cell killing in a three-day viability assay. Administration of 1 orally led to effective tumor reduction in a human-tumor xenograft mouse model of MDA-MB-231 breast cancer when dosed as a single agent. Predictions of human pharmacokinetics, using *in vivo* preclinical pharmacokinetic data and allometry or *in vitro–in vivo* extrapolation of hepatocyte stability data, suggested that 1 would exhibit moderate clearance in humans with a moderate volume of distribution. On the basis of the described properties as a whole, 1 was selected as the first compound targeting IAP proteins to enter clinic trials. Pharmacokinetics observed in humans were well behaved and consistent with preclinical predictions.

■ EXPERIMENTAL SECTION

All chemicals were purchased from commercial suppliers (Aldrich, VWR). Flash chromatography was carried out with RediSep pre-packed SiO_2 cartridges on an ISCO Companion chromatography system. NMR spectra were recorded on a Varian Inova 400 system, and referenced to tetramethylsilane. Preparative HPLC was performed on a Polaris C_{18} 5 μm column (50 × 21 mm). Low-resolution mass spectra were recorded on a Sciex 15 in ES+ mode. Final compounds were also purified on a Berger Instruments SFC system operating at 100 bar, 35 °C; column = Berger Diol 4.6 × 150 mm; with a six–minute gradient of 20–60% MeOH in CO_2 flowing 2.35 mL/min (SFCd method) or a Berger Pyridine column 4.6 × 150 mm; with a six-minute gradient of 5–50% MeOH in CO_2 flowing at 2.35 mL/min (SFCp). Purity analysis of final compounds was performed by a 20 min HPLC-MS analysis with a Chromasil C_{18} column (4.6 × 50 mm) with a gradient of 0–90% acetonitrile (containing 0.038% TFA) in 0.1% aqueous TFA (over 17 min, flow = 2 mL/min). All final compounds were purified to >95% purity.

(S)-*tert*-Butyl 2-(4-phenyl-1,2,3-thiadiazol-5-ylcarbamoyl)-pyrrolidine-1-carboxylate (12). 4-Phenyl-1,2,3-thiadiazol-5-amine (1.0 g, 5.64 mmol), Boc-L-proline (1.28 g, 5.94 mmol), EDC (1.14 g, 5.94 mmol), HOBt, (0.8 g, 5.94 mmol), and DIPEA (1.04 mL, 5.94 mmol) were dissolved in 5 mL of DMF and stirred for 24 h at room temperature. EtOAc (100 mL) was added to the solution, and the organic layer was washed with saturated aqueous $NaHCO_3$ (20 mL) and separated. The aqueous layer was extracted with two 100 mL portions of EtOAc and the organic layers combined. The combined organic layer was washed one time with saturated aqueous $NaHCO_3$ (20 mL), washed twice with saturated brine (20 mL), dried over $MgSO_4$, and concentrated to a solid residue. The crude material was purified by reverse phase HPLC to obtain compound 12 as a 2/1 mixture of rotomers (1.60 g, 76%). ^{1}H NMR (400 MHz, DMSO) δ ppm 11.90 (s, 0.66H), 11.85 (s, 0.33H), 7.68–7.75 (m 2H), 7.50–7.63 (m, 3H), 4.69 (dd, J = 8.41, 3.42 Hz, 0.33H), 4.63 (dd, J = 8.13, 4.12 Hz, 0.66H), 3.32–3.51 (m, 2H), 2.11–2.26 (m, 1H), 1.82–1.97 (m, 3H), 1.42 (s, 3H), 1.21 (s, 6H). ^{13}C NMR (100 MHz, DMSO) δ ppm 23.30, 23.94, 27.75, 28.01, 29.76, 30.89, 46.52, 46.70, 58.60, 58.73, 78.77, 79.17, 128.68, 128.74, 128.85, 128.94, 130.57, 145.40, 147.68, 152.74, 152.78, 172.37, 173.06. MS (ESI): m/z [M + H]$^+$ 375.1.

(S)-1-((S)-2-Cyclohexyl-2-((S)-2-(methylamino)propan-amido)acetyl)-N- (4-phenyl-1,2,3-thiadiazol-5-yl)pyrrolidine-2-carboxamide (1). Amide 12 (2.32 g, 6.2 mmol) was treated with 4 N
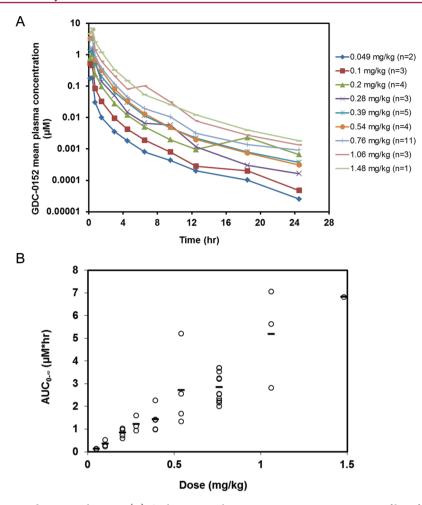
Figure 8. Compound **1** pharmacokinetics in humans. (A) Cycle 1 mean plasma concentration versus time profiles of compound **1** by cohort. (B) Plasma exposure (AUC_{inf}) of **1** plotted versus dose.

HCl/dioxane (25 mL) for 30 min, and the solution was concentrated. TEA/CH_2Cl_2 (10:90, 20 mL) was added, and the solution was stirred for 5 min and concentrated to a solid residue. Boc-L-cyclohexylglycine (1.6 g, 6.2 mmol), BOP (2.7 g, 6.2 mmol), and DIPEA (2.16 mL, 12.4 mmol) in 10 mL of DMF were added and stirred for 3 h at room temperature. EtOAc (100 mL) was added to the solution, and the organic layer was washed with saturated aqueous $NaHCO_3$ (20 mL) and separated. The aqueous layer was extracted with two 100 mL portions of EtOAc and the organic layers combined. The combined organic layer was washed one time with saturated aqueous $NaHCO_3$ (20 mL), washed twice with saturated brine (20 mL), dried over $MgSO_4$, and concentrated to a solid residue. The crude reaction mixture was treated with 25 mL of 4 N HCl/dioxane for 30 min. The solution was concentrated, TEA/CH_2Cl_2 (10:90, 20 mL) was added and stirred for 5 min, and the solution was concentrated to a solid residue. Boc-N-methylalanine (1.26, 6.2 mmol), BOP (2.7 g, 6.2 mmol), and DIPEA (2.16 mL, 12.4 mmol) in DMF (10 mL) were added, and the solution was stirred for 3 h at room temperature. EtOAc (100 mL) was added to the solution, and the organic layer was washed with saturated aqueous $NaHCO_3$ (20 mL) and separated. The aqueous layer was extracted with two 100 mL portions of EtOAc and the organic layers combined. The combined organic layer was washed one time with saturated aqueous $NaHCO_3$ (20 mL), washed twice with saturated brine (20 mL), dried over $MgSO_4$, and concentrated to a solid residue. The crude material was purified by reverse phase HPLC. The purified material was treated with 25 mL of 4 N HCl/dioxane for 30 min and the solution concentrated to a solid residue and purified by reverse phase HPLC to obtain **1** (2.28 g, 74%) ^{1}H NMR (400 MHz, CDCl$_3$) δ ppm 7.75 (d, J = 7.23 Hz, 2H), 7.62 (d, J = 9.08 Hz, 1H), 7.59 (t, J = 7.69 Hz, 2H), 7.50 (t, J = 7.38 Hz, 1H),

4.91 (dd, J = 8.08, 1.92 Hz, 1H), 4.45 (d, J = 8.23 Hz, 1H), 3.87 (q, J = 8.56 Hz, 1H), 3.58 (q, J = 5.04 Hz, 1H), 3.06 (q, J = 6.92 Hz, 1H), 2.69 (d, J = 12.46 Hz, 1H), 2.45 (s, 3H), 2.03–2.19 (m, 2H), 1.87–2.03 (m, 1H), 1.40–1.69 (m, 1H), 1.35–1.60 (m, 5H), 1.32 (d, J = 10.31 Hz, 3H), 0.79–1.02 (m, 5H). ^{13}C NMR (100 MHz, CDCl$_3$) δ ppm 175.13, 173.84, 168.92, 148.34, 144.87, 130.52, 129.20, 129.23, 128.92, 128.28, 128.27, 60.34, 59.72, 54.58, 47.99, 40.35, 35.21, 29.65, 28.17, 25.87, 25.74, 25.65, 25.63, 25.11, 19.62. MS (ESI): m/z [M + H]$^+$ 499.7

Preparation of Compounds 6a–6d. 2,2-Diphenylethylamine (5.3 g, 27 mmol) and NaCNBH$_3$ (1.7 g, 27 mmol) were added to 2-(3,5-dimethoxy-4-formylphenoxy)ethoxymethyl (DFPE) polystyrene resin (5 g, 4.5 mmol) in 1% HOAc/DMF (200 mL), and nitrogen was bubbled through the reaction mixture for 3 days at room temperature. The resin was dried and washed with DMF (2 × 100 mL) and CH_2Cl_2 (2 × 100 mL) and dried. Fmoc-Pro (4.6 g, 13.5 mmol), HATU (5.1 g, 13.5 mmol) and DIPEA (4.7 mL, 27 mmol) in 1:1 DCM/DMF (100 mL) were added to the resin, and nitrogen was bubbled through the reaction mixture for 4 h. The resin was dried and washed with DMF (2 × 100 mL) and CH_2Cl_2 (2 × 100 mL) and dried to yield Resin 3. Resin 3 was treated with 20% piperidine/DMA (100 mL) for 30 min, and the resin was dried and washed with DMF (2 × 100 mL) and CH_2Cl_2 (2 × 100 mL) and dried. Fmoc Val (4.6 g, 13.5 mmol), HBTU (5.1 g, 13.5 mmol), and DIPEA (4.7 mL, 27 mmol) were added to 1:1 DCM/DMF (100 mL), and nitrogen was bubbled through the reaction mixture for 3 h. The resin was dried and washed with DMF (2 × 100 mL) and CH_2Cl_2 (2 × 100 mL) and treated with 20% piperidine/DMA (100 mL) for 30 min. The resin was dried and washed with DMF (2 × 100 mL) and CH_2Cl_2 (2 × 100 mL) and dried to yield resin 5. The aldehyde (13.5 mmol) and NaCNBH$_3$ (0.85 g,

13.5 mmol) were added to resin 5 in 1% HOAc/DMF (100 mL) and nitrogen was bubbled through the reaction mixture for 3 days at room temperature. TFA and H$_2$O (95:5, 100 mL) were added, and nitrogen was bubbled through the solution for 1 h. The solution was concentrated to a solid residue and purified by reverse phase HPLC to yield the product.

(S)-N-(2,2-Diphenylethyl)-1-((S)-3-methyl-2-((S)-2-(methylamino)propanamido)butanoyl)pyrrolidine-2-carboxamide (6a). ^{1}H NMR (400 MHz, CD$_3$OD) δ 7.35−7.22 (m, 8H), 7.22−7.10 (m, 2H), 4.45 (t, J = 9.5 Hz, 1H), 4.28−4.19 (m, 2H), 4.05 (ddd, J = 13.4, 9.0, 7.0 Hz, 1H), 3.92−3.83 (m, 1H), 3.84−3.73 (m, 1H), 3.67−3.53 (m, 2H), 2.64 (d, J = 3.1 Hz, 3H), 2.18−2.03 (m, 1H), 2.00−1.77 (m, 3H), 1.50 (t, J = 5.6 Hz, 1H), 1.45 (d, J = 7.0 Hz, 3H), 1.05 (d, J = 6.8 Hz, 3H), 0.99 (d, J = 6.7 Hz, 3H), 0.97−0.86 (m, 1H). ^{13}C NMR (75 MHz, CD$_3$OD) δ 173.62, 172.64, 172.11, 170.80, 168.78, 168.18, 161.85, 161.40, 158.50, 156.69, 144.64, 142.38, 132.91, 128.70, 128.40, 128.34, 128.29, 128.06, 127.89, 127.47, 126.49, 126.44, 117.95, 83.38, 60.53, 60.43, 57.36, 57.17, 57.07, 56.76, 50.86, 50.58, 44.11, 43.80, 32.03, 31.89, 30.79, 30.43, 29.61, 24.80, 22.13, 18.75, 18.50, 17.54, 17.41, 15.49, 15.29. LC/MS (ESI+): *m/z* 480 [M + H].

(R)-3-((S)-2-Cyclohexyl-2-((S)-2-(methylamino)propanamido)-acetyl)-N-(2,2-diphenylethyl)thiazolidine-4-carboxamide (6b). ^{1}H NMR (400 MHz, CDCl$_3$) δ 7.34−7.23 (m, 8H), 7.20 (ddd, J = 10.1, 8.6, 6.1 Hz, 2H), 5.03 (d, J = 8.3 Hz, 1H), 4.60−4.51 (m, 1H), 4.49 (s, 2H), 4.27 (t, J = 7.9 Hz, 1H), 4.16 (dd, J = 14.0, 7.2 Hz, 1H), 3.90 (s, 1H), 3.73 (ddt, J = 8.8, 6.0, 4.3 Hz, 1H), 3.60 (d, J = 19.8 Hz, 1H), 2.91 (dd, J = 12.0, 7.2 Hz, 1H), 2.63 (d, J = 9.3 Hz, 1H), 2.55 (s, 3H), 1.66 (t, J = 24.0 Hz, 4H), 1.35 (d, J = 5.3 Hz, 3H), 1.28−1.07 (m, 4H), 1.08−0.85 (m, 3H). ^{13}C NMR (101 MHz, CD$_3$OD) δ 169.00, 168.60, 168.44, 142.63, 142.52, 128.33, 128.23, 127.85, 127.80, 126.29, 126.23, 61.73, 55.62, 55.49, 49.98, 49.42, 42.96, 33.00, 30.59, 28.41, 27.79, 25.66, 25.45, 25.34, 15.70, 15.56. LC/MS (ESI+): *m/z* 539 [M + H].

(S)-1-((S)-2-((S)-2-(Cyclopropylamino)propanamido)-3-methyl-butanoyl)-N-(2,2-diphenylethyl)pyrrolidine-2-carboxamide (6c). ^{1}H NMR (400 MHz, CD$_3$OD) δ 7.37−7.23 (m, 8H), 7.23−7.09 (m, 2H), 4.44 (t, J = 6.7 Hz, 1H), 4.30−4.17 (m, 2H), 4.10−3.93 (m, 2H), 3.88−3.75 (m, 1H), 3.69−3.50 (m, 2H), 2.89 (dt, J = 14.4, 7.2 Hz, 1H), 2.76 (dt, J = 12.7, 7.7 Hz, 1H), 2.22−2.01 (m, 1H), 2.00−1.74 (m, 3H), 1.51 (t, J = 6.3 Hz, 1H), 1.47 (d, J = 7.0 Hz, 3H), 1.13−1.01 (m, 3H), 0.98 (d, J = 6.7 Hz, 3H), 0.92 (dd, J = 10.7, 6.8 Hz, 1H), 0.77−0.61 (m, 2H), 0.43−0.25 (m, 2H). ^{13}C NMR (101 MHz, CD$_3$OD) δ 172.82, 172.74, 172.23, 170.88, 170.70, 168.93, 168.35, 142.56, 142.53, 142.41, 128.41, 128.36, 128.29, 128.06, 127.94, 127.90, 126.52, 126.49, 126.44, 60.34, 60.30, 56.96, 56.64, 55.47, 55.23, 51.14, 51.05, 50.41, 43.98, 43.75, 43.64, 31.86, 31.58, 30.19, 29.46, 24.63, 21.92, 18.56, 18.32, 17.37, 17.19, 15.63, 15.47. LC/MS (ESI+): *m/z* 538 [M + H].

(S)-1-((S)-2-((S)-2-((S)-2,3-Dihydroxypropylamino)propanamido)-3-methylbutanoyl)-N-(2,2-diphenylethyl)pyrrolidine-2-carboxamide (6d). ^{1}H NMR (400 MHz, CD$_3$OD) δ 7.36−7.24 (m, 8H), 7.23−7.12 (m, 2H), 4.49−4.40 (m, 1H), 4.32−4.17 (m, 1H), 4.09−4.00 (m, 2H), 3.92−3.86 (m, 1H), 3.79 (t, J = 14.5 Hz, 1H), 3.67−3.55 (m, 3H), 3.55−3.45 (m, 1H), 3.21−3.11 (m, 1H), 3.02−2.89 (m, 1H), 2.10 (dt, J = 14.1, 4.7 Hz, 1H), 2.01−1.77 (m, 3H), 1.52−1.47 (m, 3H), 1.44 (t, J = 6.1 Hz, 1H), 1.05 (dd, J = 6.8, 2.1 Hz, 3H), 1.00−0.96 (m, 3H), 0.93 (dd, J = 12.1, 6.8 Hz, 1H). ^{13}C NMR (101 MHz, CD$_3$OD) δ 172.84, 170.86, 169.77, 168.95, 161.54, 142.53, 128.35, 128.30, 128.07, 127.96, 127.90, 127.73, 126.50, 126.44, 67.28, 67.20, 63.94, 60.35, 57.00, 56.70, 55.84, 50.72, 50.44, 48.88, 43.75, 31.61, 30.31, 30.22, 29.46, 24.61, 21.90, 18.56, 18.32, 17.42, 17.39, 17.25, 16.56, 16.41, 15.50, 15.28. LC/MS (ESI+): *m/z* 540 [M + H].

(S)-1-((S)-2-cCyclohexyl-2-((S)-2-(methylamino)-propanamido)acetyl)-N-(2,2-diphenylethyl)pyrrolidine-2-carboxamide (10a). Boc-MeAla-Chg-Pro (8) (50 mg, 0.11 mmol) was diluted with CH$_2$Cl$_2$ (10 mL) and treated with 2, 2-diphenylethylamine (33.67 mg, 0.171 mmol), DIC (0.03 mL, 0.171 mmol), and HOBT (28 mg, 0.171 mmol). The reaction was stirred at room temperature for 1 h, and the reaction mixture was diluted with CH$_2$Cl$_2$ (100 mL) and washed with water (2 × 20 mL), and the organic layer was dried, concentrated, and purified by ISCO chromatography (50−

80% EtOAc/hexane) to yield the product. The compound was treated with 1:1 TFA and CH$_2$Cl$_2$ at room temperature for 30 min. The reaction mixture was diluted with CH$_2$Cl$_2$ (100 mL), washed with water (2 × 20 mL), and the organic layer was dried, concentrated, and purified by HPLC to yield the product. (48 mg, 85%).

^{1}H NMR (500 MHz, DMSO) δ 7.84 (dt, J = 11.0, 5.5 Hz, 1H), 7.81 (d, J = 9.0 Hz, 1H), 7.36−7.30 (m, 1H), 7.38−7.23 (m, 9H), 7.23−7.08 (m, 2H), 4.35 (dd, J = 16.9, 8.4 Hz, 1H), 4.20−4.12 (m, 2H), 3.93 (ddd, J = 22.1, 13.6, 7.5 Hz, 1H), 3.69−3.58 (m, 1H), 3.54−3.48 (m, 1H), 3.48−3.41 (m, 1H), 2.91 (q, J = 6.8 Hz, 1H), 2.13 (d, J = 10.5 Hz, 3H), 1.83−1.55 (m, 10H), 1.13 (dt, J = 11.3, 8.5 Hz, 2H), 1.06 (t, J = 9.3 Hz, 3H), 1.03−0.81 (m, 3H). ^{13}C NMR (500 MHz, DMSO) δ 173.4, 171.1, 169.3, 142.8, 129.1, 128.1, 126.3, 59.2, 54, 50.2, 46.9, 42.8, 34.2, 29.2, 28.9, 27.9, 25.9, 25.7, 25.5, 24.1, 19.1. LC/MS (ESI+): *m/z* 534 [M + H].

(S)-N-(4-Chlorobenzyl)-1-((S)-2-cyclohexyl-2-((S)-2-(methylamino)propanamido)acetyl)pyrrolidine-2-carboxamide (10b). Boc-MeAla-Chg-Pro (8) (50 mg, 0.11 mmol) was diluted with CH$_2$Cl$_2$ (10 mL), and treated with 4-chlorophenylmethanamine (24 mg, 0.171 mmol), DIC (0.03 mL, 0.171 mmol) and HOBT (28 mg, 0.171 mmol). The reaction was stirred at room temperature for 1 h, and the reaction mixture was diluted with CH$_2$Cl$_2$ (100 mL) and washed with water (2 × 20 mL), and the organic layer was dried, concentrated, and purified by ISCO chromatography (50−80% EtOAc/hexane) to yield the product. The compound was treated with 1:1 TFA and CH$_2$Cl$_2$ at room temperature for 30 min. The reaction mixture was diluted with CH$_2$Cl$_2$ (100 mL) and washed with water (2 × 20 mL), and the organic layer was dried, concentrated, and purified by HPLC to yield the product. (40 mg, 79%). ^{1}H NMR (500 MHz, DMSO) δ 8.46−8.32 (m, 1H), 7.86 (d, J = 8.9 Hz, 1H), 7.42−7.31 (m, 2H), 7.28 (t, J = 8.4 Hz, 2H), 4.41 (t, J = 8.1 Hz, 1H), 4.31 (dd, J = 8.0, 5.2 Hz, 1H), 4.27 (t, J = 6.8 Hz, 1H), 4.25−4.18 (m, 1H), 3.73 (dt, J = 9.5, 6.6 Hz, 1H), 3.59 (dt, J = 9.5, 6.9 Hz, 1H), 3.01−2.88 (m, 1H), 2.17 (d, J = 3.3 Hz, 3H), 2.12−2.02 (m, 1H), 1.97 (dd, J = 12.5, 6.1 Hz, 1H), 1.89−1.75 (m, 2H), 1.66 (ddd, J = 44.7, 26.1, 13.0 Hz, 6H), 1.19−1.11 (m, 2H), 1.08 (dd, J = 10.2, 4.9 Hz, 3H), 1.06−0.84 (m, 3H). ^{13}C NMR (500 MHz, DMSO) δ 174.1, 171.6, 169.8, 138.6, 131.1, 128.8, 128, 59.5, 59.2, 54.1, 47.1, 41.5, 34.3, 29.3, 28.9, 27.8, 25.9, 25.6, 25.5, 24.6, 19.1. LC/MS (ESI+): *m/z* 519 [M + H].

(S)-1-((S)-2-((S)-2-(Methylamino)propanamido)-2-phenylace-tyl)-N-(4-phenyl-1,2,3-thiadiazol-5-yl)pyrrolidine-2-carboxamide (14). Amide 12 (1.16 g, 3.1 mmol) was treated with 15 mL of 4 N HCl/dioxane for 30 min, and the solution was concentrated. TEA/CH$_2$Cl$_2$ (10:90, 15 mL) was added, and the solution was stirred for 5 min and concentrated to a solid residue. Boc-L-Phenylglycine (0.8 g, 3.1 mmol), 1.35 g (3.1 mmol) of BOP, and 1.08 mL (6.2 mmol) of DIPEA in 10 mL of DMF were added and stirred for 3 h at room temperature. One hundred milliliters of EtOAc was added to the solution, and the organic layer was washed with saturated aqueous NaHCO$_3$ (20 mL) and separated. The aqueous layer was extracted with two 100 mL portions of EtOAc and the organic layers combined. The combined organic layer was washed one time with saturated aqueous NaHCO$_3$ (20 mL), washed twice with saturated brine (20 mL), dried over MgSO$_4$, and concentrated to a solid residue. The crude reaction mixture was treated with 25 mL of 4 N HCl/dioxane for 30 min. The solution was concentrated, TEA/CH$_2$Cl$_2$ (10:90, 15 mL) was added and stirred for 5 min, and the solution was concentrated to a solid residue. Boc-N-methylalanine (0.63 g, 3.1 mmol), BOP (1.35 g, 3.1 mmol), and DIPEA (1.08 mL, 12.4 mmol) in 10 mL of DMF were added, and the solution was stirred for 3 h at room temperature. EtOAc (100 mL) was added to the solution, and the organic layer was washed with saturated aqueous NaHCO$_3$ (20 mL) and separated. The aqueous layer was extracted with two 100 mL portions of EtOAc and the organic layers combined. The combined organic layer was washed one time with saturated aqueous NaHCO$_3$ (20 mL), washed twice with saturated brine (20 mL), dried over MgSO$_4$, and concentrated to a solid residue. The crude material was purified by reverse phase HPLC. The purified material was treated with 25 mL of 4 N HCl/dioxane for 30 min, the solution concentrated to a solid residue, and purified by reverse phase HPLC to obtain 14 (1.19 g, 78%). ^{1}H NMR (400 MHz, CDCl$_3$)

δ 7.88−7.76 (m, 2H), 7.74−7.61 (m, 2H), 7.58−7.47 (m, 1H), 7.29−7.21 (m, 1H), 7.22−7.12 (m, 2H), 7.04−6.92 (m, 2H), 5.54 (s, 1H), 5.02−4.89 (m, 1H), 3.78−3.58 (m, 1H), 3.24 (t, J = 7.6 Hz, 1H), 3.13 (q, J = 6.9 Hz, 1H), 2.60−2.51 (m, 1H), 2.47 (s, 3H), 2.12−1.80 (m, 3H), 1.25 (d, J = 6.9 Hz, 3H). ^{13}C NMR (101 MHz, CD_3OD) δ 171.92, 168.96, 167.87, 167.62, 167.27, 157.71, 157.48, 138.10, 136.06, 128.62, 128.56, 128.24, 128.04, 127.88, 127.52, 56.23, 55.79, 54.67, 46.76, 46.66, 31.55, 31.15, 30.49, 29.16, 24.61, 21.83, 20.96, 16.09, 15.38. LC/MS (ESI+): m/z 493 [M + H].

X-ray Crystallography. Compound **1** was soaked into crystals of the chimeric BIR domain MLXBIR3SG in complex with the peptide AVPW using protocols described previously.[50] Data for the MLXBIR3SG/**1** complex were collected at beamline 9−1 of the Stanford Synchrotron Radiation Lightsource. The starting models for refinement of these structures were derived from a 1.3-Å resolution structure of a different peptidomimetic complex (details to be published elsewhere), which was stripped of the peptidomimetic antagonist molecule and all water molecules within 10 Å of it. After one round of refinement of the antagonist-free model, **1** was built into clear difference electron density visible in $F_o − F_c$ maps. New water molecules were picked automatically using the program Arp/wArp,[55] and the entire new complex model was subjected to several rounds of positional, anisotropic B-factor, and translation−libration−screw (TLS) refinement using Refmac5.[56] The structure has been deposited with the Protein Data Bank and assigned the accession code 3UW5.

DNA encoding for a chimeric human cIAP1 composed of cIAP1 residues 266−354 with the mutation C309S and residues 344−354 replaced by residues 336−348 of XIAP (hereafter referred to as cXBIR3CS) was subcloned into the pET15b vector and expressed in *E. coli* strain BL-21(DE3) grown in TB media supplemented with 1% glycerol and 50 μM zinc acetate. Cultures were transformed and grown at 37 °C until an OD_{600} of 2.0, induced with 0.5 mM IPTG, grown overnight at 16 °C, harvested by centrifugation, and lysed in 50 mM Tris-HCl at pH 8.3, 300 mM NaCl, 0.5 mM TCEP, and 5 mM imidazole with 2 Complete Protease Inhibitor tablets (Roche). Soluble cXBIR3CS was purified using Ni-NTA agarose (Qiagen) affinity chromatography and eluted in 50 mM Tris-HCl at pH 8.3, 300 mM NaCl, 0.5 mM TCEP, and 300 mM imidazole. Thrombin was added to the cXBIR3CS-containing fractions followed by dialysis for 36 h at 4 °C against 20 mM Tris-HCl at pH 8.5, 200 mM NaCl, 0.2 mM TCEP, 2 mM $CaCl_2$ to remove the His-tag. Uncleaved material was removed by repassage over the Ni-NTA agarose column. The flow through was concentrated and loaded onto a S-75 sizing column pre-equilibrated in 20 mM Tris-HCl at pH 8.3, 200 mM NaCl, and 0.2 mM TCEP. Purified cXBIR3CS was concentrated to 4 mg/mL in 50 mM HEPES, pH 7.2, 300 mM NaCl, and 0.2 mM TCEP. Compound **1** (50 mM stock solution in DMSO) was added to a final concentration of 1 mM. The cXBIR3CS−compound **1** complex was crystallized by vapor diffusion from hanging drops containing equal volumes of protein and reservoir solution (0.1 M Tris-HCl pH 8.6, and 0.5 M magnesium formate). Crystals were cryo-protected in 0.1 M Tris-HCl at pH 8.5, 0.5 M magnesium formate, and 3 M sodium formate. A data set was measured at the Advanced Light Source (Berkeley) beamline 5.0.2 and processed with the HKL suite of programs. The structure was solved by molecular replacement with the program Phaser using the BIR3 domain of cIAP2 (PDB code 2UVL) as a search model and was refined with Refmac5. The structure has been deposited with the Protein Data Bank and assigned the accession code 3UW4.

Refinement statistics for the complex structures are in Table S1 (Supporting Information).

Binding Assays. Initial polarization experiments were performed in order to determine dissociation constants (K_d) between IAP protein BIR domains and fluorescent probes. Samples for fluorescence polarization affinity measurements were prepared by the addition of serial dilutions of MLXBIR3SG, XIAP-BIR3, XIAP-BIR2, cIAP1-BIR3, cIAP2-BIR3 in polarization buffer (50 mM Tris [pH 7.2], 120 mM NaCl, 1% bovine globulins, 5 mM DTT, and 0.05% octylglucoside) to 5 nM 5-carboxyflourescein (5-FAM)-conjugated AVP-diphenylala-nine-AKK (AVP-diPhe-FAM) or serial dilutions of cIAP1-BIR2 and cIAP2-BIR2 in polarization buffer to 5 nM AVPFAK(5-FAM)K (Hid-FAM). The reactions were read after an incubation time of 30 min at room temperature with standard cutoff filters for the fluorescein fluorophore (λ_{ex} = 485 nm; λ_{em} = 530 nm) in 384-well black HE96 plates (Molecular Devices Corp.). Fluorescence polarization values were plotted as a function of the protein concentration, and the EC_{50} values were obtained by fitting the data to a 4-parameter equation using KaleidaGraph software (Synergy software, Reading, PA). The apparent K_d values were determined from the EC_{50} values.

Inhibition constants (K_i) for the antagonists were determined by the addition of the IAP protein constructs to wells containing serial dilutions of the antagonists or the peptide AVPW and the Hid-FAM probe or AVP-diPhe-FAM probe, as appropriate, in the polarization buffer. Samples were read after a 30-min incubation. Fluorescence polarization values were plotted as a function of the antagonist concentration, and the IC_{50} values were obtained by fitting the data to a 4-parameter equation using KaleidaGraph software. K_i values for the antagonists were determined from the IC_{50} values.[57]

Cells, Reagents, and Co-Immunoprecipatation. HEK293T, melanoma SK-MEL28 and A2058, and breast cancer MDA-MB-231 cells were obtained from ATCC and maintained in the recommended media. Antibodies against Myc (Upstate), Flag (SIGMA), c-IAP1 (R & D Systems), caspase-9 (Cell Signaling), and Smac (ProSci) were purchased, and ML-IAP antibody was described previously.[58] zVAD was purchased from Biomol.

HEK293T cells were transiently transfected with the indicated constructs, and 40 h after transfection, the cells were lysed in NP40 lysis buffer. Lysates were incubated with 0, 1, 10, or 100 mM concentrations of the indicated test materials for 2 h, followed by immunoprecipitation with anti-Flag or anti-Myc antibodies for 3 h, SDS−PAGE and immuno-blotting with anti-Flag, anti-Myc, anti-SMAC, and anticaspase-9 antibodies.

SK-MEL28 cells were treated with Gemcitabine (0.5 mM) and **1** (0.5 mM) for 20 h in the presence of the caspase inhibitor, zVAD (10 mM). At that time, the cells were lysed in NP40 lysis buffer, immunoprecipitated with the anti-Smac antibody, resolved on SDS−PAGE, and immuno-blotted with anti-ML-IAP and anti-Smac antibodies.

Cell Viability and Caspase Activation Assays. Human breast carcinoma MDA-MB-231 were obtained from ATCC. Normal human mammary epithelial cells (HMECs) were obtained from Cambrex Corp. Cells were dissociated from tissue culture flasks by incubation with Accutase (Innovative Cell Technology Inc.) for 5−10 min. Detached cells were washed with phosphate-buffered saline (PBS) and were resuspended in assay media (MDA-MB-231 cells: RPMI1640 supplemented with 10% fetal bovine serum [Sigma-Aldrich] and 2 mM L-glutamine [GlutaMAX-1; Gibco/Invitrogen Corp.]) or culture media (HMECs: MEBM with MEGM SingleQuots provided by Cambrex Corp.). Cells were placed in tissue culture-treated, white-wall (Corning, Inc.) or black-wall (PE Biosystems), clear-bottom, 96-well plates at 1 × 10^4 cells/well in a volume of 50 μL. The plates were incubated at 37 °C and 5% CO_2 overnight, the media was removed, and **1** or its enantiomer was added to the assay media. Cells cultured in white-wall, clear-bottom plates were incubated at 37 °C and 5% CO_2 for 3 days before cell viability was measured using the CellTiter-Glo luminescent cell viability assay kit (Promega Corp.) according to the manufacturer's instructions. Cells seeded in black-wall, clear-bottom plates were incubated at 37 °C and 5% CO_2 for 3−24 h before caspase-3 and -7 activities were assessed using the Apo-ONE homogeneous caspase-3/7 assay kit (Promega Corp.) according to the manufacturer's instructions.

Tumor Xenograft Study. All procedures involving animals were performed in accordance with the guidelines of the Genentech Institutional Animal Care and Use Committee. Human breast cancer MDA-MB-231 cells were obtained from American Type Culture Collection (Manassas, VA). Cells were resuspended in PBS, and the cell suspension was mixed 1:1 with Matrigel (BD Biosciences). The cells (1.5 × 10^7) were then implanted subcutaneously into the right flank of 130 female nude mice (Charles River Laboratories, Hollister, CA) aged 6−8 weeks. Tumor volumes were calculated using the mean

diameter measured with vernier calipers using the formula $v = 0.5 \times a \times b^2$, where a and b are the largest and smallest perpendicular tumor diameters, respectively. Ten mice with the appropriate mean tumor volume were assigned randomly to each of six groups. The mean tumor volume ± the standard error of the mean (SEM) for all six groups was 168 ± 3 mm^3 at the initiation of treatment (day 0). Mice were dosed with **1** or vehicle (PBS) by oral gavage with a dose volume of 4.0 mL/kg, according to the schedule indicated in Figure 6. The mice were observed on each day of the study, and tumor volumes and body weights were measured twice each week. Percent tumor growth inhibition was calculated using the formula % TGI = $100 \times (1 -$ tumor volume$_{dose}$/tumor volume$_{vehicle}$).

Pharmacokinetic Studies in Mouse, Rat, Dog, and Monkey. Compound **1** was intravenously administered to Sprague–Dawley rats ($n = 3$ per dose level), Beagle dogs ($n = 3$ at 1 mg/kg and $n = 2$ at 20 mg/kg), and cynomolgus monkeys ($n = 3$ per dose level) at doses of 1 and 20 mg/kg. Serial plasma samples were collected following dosing up to 24 h postdose. In nude mice ($n = 27$ per dose level), **1** was administered intravenously at doses of 1 and 100 mg/kg. Mice plasma samples ($n = 3$ per time point) were collected for up to 24 h postdose. Compound **1** plasma concentrations were determined using LC-MS/MS. Pharmacokinetic parameters were determined using noncompartmental analysis.[59]

Plasma Protein Binding. The plasma protein binding of **1** was determined at 0.1, 1, 10, and 100 μM by equilibrium dialysis using a 96-well equilibrium dialysis block (HTDialysis LLC, Gales Ferry, CT, USA). Compound **1** (mix of unlabeled + ^{14}C-labeled) in pooled plasma from female CD-1 mice, male rats, female rabbits, male dogs, male monkeys, and male humans ($n \geq 3$ for all species) was obtained. The radioactivity of the postdialysis buffer and plasma samples were quantified by liquid scintillation counter. The percent unbound fraction in plasma was calculated by dividing the radiation counts in the postdialysis buffer side by the radiation counts in the postdialysis plasma side and multiplying by 100.

■ BLOOD PLASMA PARTITIONING

Blood–plasma partitioning was assessed at total (unlabeled + ^{14}C-labeled) **1** concentrations of 0.1, 1, 10, and 100 μM in pooled blood from female CD-1 mice, male rats, female rabbits, male dogs, male monkeys, and male humans ($n \geq 3$ for all species). The blood samples were incubated at 37 °C for 0.5 h. Radioactivity in blood and plasma samples was quantified by liquid scintillation counter.

Hepatocyte Stability Assay and Hepatic Clearance Prediction. Compound **1** (1 μM) was incubated with human cryopreserved hepatocytes (0.5×10^6 cells/mL) at 37 °C for 0, 1, 2, and 3 h. Concentrations were assessed by LC/MS/MS. Intrinsic clearance based upon hepatocyte stability data was determined using a substrate depletion method and scaled to hepatic clearance using the well-stirred model.[60]

Allometric Scaling. Allometric scaling based on maximum life expectancy potential (MLP) and simple allometric scaling were used to predict human plasma clearance and volume of distribution, respectively.[61]

Human Pharmacokinetics. A phase Ia, first-in-human, open-label, multicenter, standard dose-escalation study (3 + 3 design) of **1** was conducted in patients with locally advanced or metastatic solid malignancies or non-Hodgkin's lymphoma without leukemic phase. Patients were given **1** doses of 0.049, 0.1, 0.2, 0.28, 0.39, 0.54, 0.76, 1.06, or 1.48 mg/kg as a 0.5 h intravenous infusion every 14 days. Serial plasma samples were collected at predetermined time points up to approximately 24 h postdose during the first two cycles. Compound **1** plasma concentrations were measured using LC/MS/MS. Pharmacokinetic parameters were calculated using noncompartmental analysis.[62]

■ ASSOCIATED CONTENT

⬤ Supporting Information

X-ray data collection and refinement statistics, summary of clinical pharmacokinetics parameters for **1** from day 1 cycle 1, and immunoprecipitation and immunoblotting of melanoma SK-MEL28 cells. This material is available free of charge via the Internet at http://pubs.acs.org.

Accession Codes

Compound **1**/cXBIR3CS, 3UW4; compound **1**/MLXBIR3SG, 3UW5.

■ AUTHOR INFORMATION

Corresponding Author

*(J.A.F.) Phone: 650-225-6437. E-mail: jflygare@gene.com. (W.J.F.) Phone: 650-225-6372. E-mail: fairbro@gene.com.

Notes

The authors declare no competing financial interest.

■ ABBREVIATIONS USED

IAP, inhibitor of apoptosis; XIAP, X chromosome-linked inhibitor of apoptosis; ML-IAP, melanoma inhibitor of apoptosis; RIP, receptor interacting protein; Smac, second mitochondria-derived activator of caspases; DIABLO, Direct IAP binding protein with low pI; BIR, baculoviral IAP repeat domain; HATU, 2-(1H-7-azabenzotriazol-1-yl)--1,1,3,3-tetramethyl uronium hexafluorophosphate methanaminium; DIPEA, diisopropylethylamine; BOP, benzotriazol-1-yloxytris-(dimethylamino)-phosphonium hexafluorophosphate; HBTU, O-benzotriazole-N,N,N',N'-tetramethyl-uronium-hexafluorophosphate; HOBt, N-hydroxybenzotriazole; ADME, absorption, distribution, metabolism, and excretion; DIC, N,N'-diisopropylcarbodiimide; EDC, 1-(3-dimethylaminopropyl)-3-ethylcarbodiimide; PBS, phosphate-buffered saline; IV, intravenous; PK, pharmacokinetic; AUC, area under the curve; DFPE, 2-(3,5-dimethoxy-formylphenoxy)ethyl polystyrene; HOBt, N-hydroxybenzotriazole; DMF, dimethylformamide

■ REFERENCES

(1) Hunter, A. M.; LaCasse, E. C.; Korneluk, R. G. The inhibitors of apoptosis (IAPs) as cancer targets. *Apoptosis* **2007**, *12*, 1543−1568.

(2) Imoto, I.; Tsuda, H.; Hirasawa, A.; Miura, M.; Sakamoto, M.; Hirohashi, S.; Inazawa, J. Expression of cIAP1, a target for 11q22 amplification, correlates with resistance of cervical cancers to radiotherapy. *Cancer Res.* **2002**, *62*, 4860−4866.

(3) Imoto, I.; Yang, Z. Q.; Pimkhaokham, A.; Tsuda, H.; Shimada, Y.; Imamura, M.; Ohki, M.; Inazawa, J. Identification of cIAP1 as a candidate target gene within an amplicon at 11q22 in esophageal squamous cell carcinomas. *Cancer Res.* **2001**, *61*, 6629–6634.

(4) Vucic, D.; Stennicke, H. R.; Pisabarro, M. T.; Salvesen, G. S.; Dixit, V. M. ML-IAP, a novel inhibitor of apoptosis that is preferentially expressed in human melanomas. *Curr. Biol.* **2000**, *10*, 1359–1366.

(5) Yang, L.; Cao, Z.; Yan, H.; Wood, W. C. Coexistence of high levels of apoptotic signaling and inhibitor of apoptosis proteins in human tumor cells: implication for cancer specific therapy. *Cancer Res.* **2003**, *63*, 6815–6824.

(6) Flygare, J. A.; Vucic, D. Development of novel drugs targeting inhibitors of apoptosis. *Future Oncol.* **2009**, *5* (2), 141–144.

(7) Vucic, D.; Fairbrother, W. J. The inhibitor of apoptosis proteins as therapeutic targets in cancer. *Clin. Cancer Res.* **2007**, *13*, 5995–6000.

(8) Fischer, U.; Schulze-Osthoff, K. Apoptosis-based therapies and drug targets. *Cell Death Differ.* **2005**, *12*, 942–961.

(9) Wright, C. W.; Duckett, C. S. Reawakening the cellular death program in neoplasia through the therapeutic blockade of IAP function. *J. Clin. Invest.* **2005**, *115*, 2673–2678.

(10) Schimmer, A. D. Inhibitor of apoptosis proteins: translating basic knowledge into clinical practice. *Cancer Res.* **2004**, *64*, 7183–7190.

(11) Nachmias, B.; Ashhab, Y.; Ben-Yehuda, D. The inhibitor of apoptosis protein family (IAPs): an emerging therapeutic target in cancer. *Semin. Cancer Biol.* **2004**, *14*, 231–243.

(12) Liston, P.; Fong, W. G.; Korneluk, R. G. The inhibitors of apoptosis: there is more to life than Bcl2. *Oncogene* **2003**, *22*, 8568–8580.

(13) Salvesen, G. S.; Duckett, C. S. IAP proteins: blocking the road to death's door. *Nat. Rev. Mol. Cell Biol.* **2002**, *3*, 401–410.

(14) Asselin, E.; Mills, G. B.; Tsang, B. K. XIAP regulates Akt activity and caspase-3-dependent cleavage during cisplatin-induced apoptosis in human ovarian epithelial cancer cells. *Cancer Res.* **2001**, *61*, 1862–1868.

(15) Bertrand, M. J. M.; Milutinovic, S.; Dickson, K. M.; Ho, W. C.; Boudreault, A.; Durkin, J.; Gillard, J. W.; Jaquith, J. B.; Morris, S. J.; Barker, P. A. cIAP1 and cIAP2 facilitate cancer cell survival by functioning as E3 ligases that promote RIP1 ubiquitination. *Mol. Cell* **2008**, *30*, 689–700.

(16) Birkey Reffey, S.; Wurthner, J. U.; Parks, W. T.; Roberts, A. B.; Duckett, C. S. X-linked inhibitor of apoptosis protein functions as a cofactor in transforming growth factor-beta signaling. *J. Biol. Chem.* **2001**, *276*, 26542–26549.

(17) Chu, Z. L.; McKinsey, T. A.; Liu, L.; Gentry, J. J.; Malim, M. H.; Ballard, D. W. Suppression of tumor necrosis factor-induced cell death by inhibitor of apoptosis c-IAP2 is under NF-κB control. *Proc. Natl. Acad. Sci. U.S.A.* **1997**, *94*, 10057–10062.

(18) Dogan, T.; Harms, G. S.; Hekman, M.; Karreman, C.; Oberoi, T. K.; Alnemri, E. S.; Rapp, U. R.; Rajalingam, K. X-linked and cellular IAPs modulate the stability of C-RAF kinase and cell motility. *Nat. Cell Biol.* **2008**, *10*, 1447–1455.

(19) Hofer-Warbinek, R.; Schmid, J. A.; Stehlik, C.; Binder, B. R.; Lipp, J.; de Martin, R. Activation of NF-κB by XIAP, the X chromosome-linked inhibitor of apoptosis, in endothelial cells involves TAK1. *J. Biol. Chem.* **2000**, *275*, 22064–22068.

(20) Mahoney, D. J.; Cheung, H. H.; Mrad, R. L.; Plenchette, S.; Simard, C.; Enwere, E.; Arora, V.; Mak, T. W.; Lacasse, E. C.; Waring, J.; Korneluk, R. G. Both cIAP1 and cIAP2 regulate TNFα-mediated NF-κB activation. *Proc. Natl. Acad. Sci. U.S.A.* **2008**, *105*, 11778–11783.

(21) Sanna, M. G.; da Silva Correia, J.; Ducrey, O.; Lee, J.; Nomoto, K.; Schrantz, N.; Deveraux, Q. L.; Ulevitch, R. J. IAP suppression of apoptosis involves distinct mechanisms: the TAK1/JNK1 signaling cascade and caspase inhibition. *Mol. Cell. Biol.* **2002**, *22*, 1754–1766.

(22) Varfolomeev, E.; Blankenship, J. W.; Wayson, S. M.; Fedorova, A. V.; Kayagaki, N.; Garg, P.; Zobel, K.; Dynek, J. N.; Elliott, L. O.;

(23) Wallweber, H. J. A.; Flygare, J. A.; Fairbrother, W. J.; Deshayes, K.; Dixit, V. M.; Vucic, D. IAP antagonists induce autoubiquitination of c-IAPs, NF-κB activation, and TNFα-dependent apoptosis. *Cell* **2007**, *131*, 669–681.

(23) Varfolomeev, E.; Goncharov, T.; Fedorova, A. V.; Dynek, J. N.; Zobel, K.; Deshayes, K.; Fairbrother, W. J.; Vucic, D. c-IAP1 and c-IAP2 are critical mediators of tumor necrosis factor alpha (TNF α)-induced NF-κB activation. *J. Biol. Chem.* **2008**, *283*, 24295–24299.

(24) Xu, L.; Zhu, J.; Hu, X.; Zhu, H.; Kim, H. T.; LaBaer, J.; Goldberg, A.; Yuan, J. c-IAP1 cooperates with Myc by acting as a ubiquitin ligase for Mad1. *Mol. Cell* **2007**, *28*, 914–922.

(25) Zhao, Y.; Conze, D. B.; Hanover, J. A.; Ashwell, J. D. Tumor necrosis factor receptor 2 signaling induces selective c-IAP1-dependent ASK1 ubiquitination and terminates mitogen-activated protein kinase signaling. *J. Biol. Chem.* **2007**, *282*, 7777–7782.

(26) Varfolomeev, E.; Vucic, D. (Un)expected roles of c-IAPs in apoptotic and NFκB signaling pathways. *Cell Cycle* **2008**, *7*, 1511–1521.

(27) Du, C.; Fang, M.; Li, Y.; Li, L.; Wang, X. Smac, a mitochondrial protein that promotes cytochrome c-dependent caspase activation by eliminating IAP inhibition. *Cell* **2000**, *102*, 33–42.

(28) Verhagen, A. M.; Ekert, P. G.; Pakusch, M.; Silke, J.; Connolly, L. M.; Reid, G. E.; Moritz, R. L.; Simpson, R. J.; Vaux, D. L. Identification of DIABLO, a mammalian protein that promotes apoptosis by binding to and antagonizing IAP proteins. *Cell* **2000**, *102*, 43–53.

(29) Flygare, J.; Fairbrother, W. Small-molecule pan-IAP antagonists: a patent review. *Expert Opin. Ther. Pat.* **2010**, *20*, 251–267.

(30) Deveraux, Q. L.; Leo, E.; Stennicke, H. R.; Welsh, K.; Salvesen, G. S.; Reed, J. C. Cleavage of human inhibitor of apoptosis protein XIAP results in fragments with distinct specificities for caspases. *EMBO J.* **1999**, *18*, 5242–5251.

(31) Shiozaki, E. N.; Chai, J.; Rigotti, D. J.; Riedl, S. J.; Li, P.; Srinivasula, S. M.; Alnemri, E. S.; Fairman, R.; Shi, Y. Mechanism of XIAP-mediated inhibition of caspase-9. *Mol. Cell* **2003**, *2*, 519–527.

(32) Srinivasula, S. M.; Hegde, R.; Saleh, A.; Datta, P.; Shiozaki, E.; Chai, J.; Lee, R. A.; Robbins, P. D.; Fernandes-Alnemri, T.; Shi, Y.; Alnemri, E. S. A conserved XIAP-interaction motif in caspase-9 and Smac/DIABLO regulates caspase activity and apoptosis. *Nature* **2001**, *410*, 112–116.

(33) Sun, C.; Cai, M.; Meadows, R. P.; Xu, N.; Gunasekera, A. H.; Herrmann, J.; Wu, J. C.; Fesik, S. W. NMR structure and mutagenesis of the third Bir domain of the inhibitor of apoptosis protein XIAP. *J. Biol. Chem.* **2000**, *275*, 33777–33781.

(34) Chai, J.; Du, C.; Wu, J. W.; Kyin, S.; Wang, X.; Shi, Y. Structural and biochemical basis of apoptotic activation by Smac/DIABLO. *Nature* **2000**, *406*, 855–862.

(35) Huang, Y.; Park, Y. C.; Rich, R. L.; Segal, D.; Myszka, D. G.; Wu, H. Structural basis of caspase inhibition by XIAP: differential roles of the linker versus the BIR domain. *Cell* **2001**, *104*, 781–790.

(36) Riedl, S. J.; Renatus, M.; Schwarzenbacher, R.; Zhou, Q.; Sun, C.; Fesik, S. W.; Liddington, R. C.; Salvesen, G. S. Structural basis for the inhibition of caspase-3 by XIAP. *Cell* **2001**, *104*, 791–800.

(37) Sun, C.; Cai, M.; Gunasekera, A. H.; Meadows, R. P.; Wang, H.; Chen, J.; Zhang, H.; Wu, W.; Xu, N.; Ng, S. C.; Fesik, S. W. NMR structure and mutagenesis of the inhibitor-of-apoptosis protein XIAP. *Nature* **1999**, *6755*, 818–822.

(38) Takahashi, R.; Deveraux, Q.; Tamm, I.; Welsh, K.; Assa-Munt, N.; Salvesen, G. S.; Reed, J. C. A single BIR domain of XIAP sufficient for inhibiting caspases. *J. Biol. Chem.* **1998**, *273*, 7787–7790.

(39) Silke, J.; Hawkins, C. J.; Ekert, P. G.; Chew, J.; Day, C. L.; Pakusch, M.; Verhagen, A. M.; Vaux, D. L. The anti-apoptotic activity of XIAP is retained upon mutation of both the caspase 3- and caspase 9-interacting sites. *J. Cell Biol.* **2002**, *157*, 115–124.

(40) Liu, Z.; Sun, C.; Olejniczak, E. T.; Meadows, R. P.; Betz, S. F.; Oost, T.; Herrmann, J.; Wu, J. C.; Fesik, S. W. Structural basis for binding of Smac/DIABLO to the XIAP BIR3 domain. *Nature* **2000**, *408*, 1004–1008.

(41) Cai, Q.; Sun, H.; Peng, Y.; Lu, J.; Nikolovska-Coleska, Z.; McEachern, D.; Liu, L.; Qiu, S.; Yang, C.-Y.; Miller, R.; Yi, H.; Zhang, T.; Sun, D.; Kang, S.; Guo, M.; Leopold, L.; Yang, D.; Wang, S. A potent and orally active antagonist (SM-406/AT-406) of multiple inhibitor of apoptosis proteins (IAPs) in clinical development for cancer treatment. *J. Med. Chem.* **2011**, *54*, 2714–2726.

(42) Li, L.; Thomas, R. M.; Suzuki, H.; De Brabander, J. K.; Wang, X.; Harran, P. G. A small molecule Smac mimic potentiates TRAIL- and TNFα-mediated cell death. *Science* **2004**, *305*, 1471–1474.

(43) Oost, T. K.; Sun, C.; Armstrong, R. C.; Al-Assaad, A. S.; Betz, S. F.; Deckwerth, T. L.; Ding, H.; Elmore, S. W.; Meadows, R. P.; Olejniczak, E. T. Discovery of potent antagonists of the antiapoptotic protein XIAP for the treatment of cancer. *J. Med. Chem.* **2004**, *47*, 4417–4426.

(44) Sun, H.; Liu, L.; Lu, J.; Bai, L.; Li, X.; Nikolovska-Coleska, Z.; McEachern, D.; Yang, C.-Y.; Qiu, S.; Yi, H.; Sun, D.; Wang, S. Potent bivalent Smac mimetics: effect of the linker on binding to inhibitor of apoptosis proteins (IAPs) and anticancer activity. *J. Med. Chem.* **2011**, *54*, 3306–3318.

(45) Sun, H.; Lu, J.; Liu, L.; Yi, H.; Qiu, S.; Yang, C. Y.; Deschamps, J. R.; Wang, S. Nonpeptidic and potent small-molecule inhibitors of cIAP-1/2 and XIAP proteins. *J. Med. Chem.* **2010**, *53*, 6361–6367.

(46) Wang, S. Design of Small-Molecule Smac Mimetics as IAP Antagonists. *Small-Mol. Inhibit. Protein-Protein Interact.* **2011**, 89–113.

(47) Zuckermann, R. N.; Kerr, J. M.; Kent, S. B. H.; Moos, W. H. Efficient method for the preparation of peptoids [oligo(N-substituted glycines)] by submonomer solid-phase synthesis. *J. Am. Chem. Soc.* **1992**, *114*, 10646–10647.

(48) Cohen, F.; Alicke, B.; Elliott, L. O.; Flygare, J. A.; Goncharov, T.; Keteltas, S. F.; Franklin, M. C.; Frankovitz, S.; Stephan, J. P.; Tsui, V. Orally bioavailable antagonists of inhibitor of apoptosis proteins based on an azabicyclooctane scaffold. *J. Med. Chem.* **2009**, *52*, 1723–1730.

(49) Franklin, M. C.; Kadkhodayan, S.; Ackerly, H.; Alexandru, D.; Distefano, M. D.; Elliott, L. O.; Flygare, J. A.; Mausisa, G.; Okawa, D. C.; Ong, D. Structure and function analysis of peptide antagonists of melanoma inhibitor of apoptosis (ML-IAP). *Biochemistry* **2003**, *42*, 8223–8231.

(50) Zobel, K.; Wang, L.; Varfolomeev, E.; Franklin, M. C.; Elliott, L. O.; Wallweber, H. J. A.; Okawa, D. C.; Flygare, J. A.; Vucic, D.; Fairbrother, W. J.; Deshayes, K. Design, synthesis, and biological activity of a potent Smac mimetic that sensitizes cancer cells to apoptosis by antagonizing IAPs. *ACS Chem. Biol.* **2006**, *1*, 525–533.

(51) Cohen, F.; Koehler, M. F. T.; Bergeron, P.; Elliott, L. O.; Flygare, J. A.; Franklin, M. C.; Gazzard, L.; Keteltas, S. F.; Lau, K.; Ly, C. Q.; Tsui, V.; Fairbrother, W. J. Antagonists of inhibitor of apoptosis proteins based on thiazole amide isosteres. *Bioorg. Med. Chem. Lett.* **2010**, *20*, 2229–2233.

(52) Ndubaku, C.; Varfolomeev, E.; Wang, L.; Zobel, K.; Lau, K.; Elliott, L. O.; Maurer, B.; Fedorova, A. V.; Dynek, J. N.; Koehler, M.; Hymowitz, S. G.; Tsui, V.; Deshayes, K.; Fairbrother, W. J.; Flygare, J. A.; Vucic, D. Antagonism of c-IAP and XIAP proteins is required for efficient induction of cell death by small-molecule IAP antagonists. *ACS Chem. Biol.* **2009**, *4*, 557–566.

(53) Vucic, D.; Franklin, M. C.; Wallweber, H. J. A.; Das, K.; Eckelman, B. P.; Shin, H.; Elliott, L. O.; Kadkhodayan, S.; Deshayes, K.; Salvesen, G. S.; Fairbrother, W. J. Engineering ML-IAP to produce an extraordinarily potent caspase 9 inhibitor: implications for Smac-dependent anti-apoptotic activity of ML-IAP. *Biochem. J.* **2005**, *385*, 11–20.

(54) Dynek, J. N.; Goncharov, T.; Dueber, E. C.; Fedorova, A. V.; Izrael-Tomasevic, A.; Phu, L.; Helgason, E.; Fairbrother, W. J.; Deshayes, K.; Kirkpatrick, D. S.; Vucic, D. c-IAP1 and UbcH5 promote K11-linked polyubiquitination of RIP1 in TNF signalling. *EMBO J.* **2010**, *29*, 4198–4209.

(55) Perrakis, A.; Harkiolaki, M.; Wilson, K. S.; Lamzin, V. S. ARP/wARP and molecular replacement. *Acta Crystallogr., Sect. D* **2001**, *57*, 1445–1450.

(56) Murshudov, G. N.; Vagin, A. A.; Dodson, E. J. Refinement of macromolecular structures by the maximum-likelihood method. *Acta Crystallogr., Sect. D* **1997**, *53*, 240–255.

(57) Keating, S.; Marsters, J.; Beresini, M.; Ladner, C.; Zioncheck, K.; Clark, K.; Arellano, F.; Bodary, S. Putting the pieces together: Contribution of fluorescence polarization assays to small molecule lead optimization. *In-Vitro Diagn. Instrum.* **2000**, *1* (7), 128–137.

(58) Dynek, J. N.; Chan, S. M.; Liu, J. F.; Zha, J. P.; Fairbrother, W. J.; Vucic, D. Microphthalmia-associated transcription factor is a critical transcriptional regulator of melanoma inhibitor of apoptosis in melanomas. *Cancer Res.* **2008**, *68*, 3124–3132.

(59) Gilbaldi, M.; Perrier, D. *Pharmacokinetics*, 2nd ed.; Marcel Dekker Inc.: New York, 1982.

(60) Obach, R. S.; Baxter, J. G.; Liston, T. E.; Silber, B. M.; Jones, B. C.; MacIntyre, F.; Rance, D. J.; Wastall, P. The prediction of human pharmacokinetic parameters from preclinical and in vitro metabolism data. *J. Pharmacol. Exp. Ther.* **1997**, *283*, 46–58.

(61) Mahmood, I.; Balian, J. D. Interspecies scaling: Predicting clearance of drugs in humans. Three different approaches. *Xenobiotica* **1996**, *26*, 887–895.

(62) Perrier, D.; Mayersohn, M. Non-compartmental determination of the steady-state volume of distribution for any mode of administration. *J. Pharm. Sci.* **1982**, *71* (3), 372–373.

(63) Keating, S. M.; Marsters, J.; Beresini, M.; Ladner, C.; Zioncheck, K.; Clark, K.; Arellano, F.; Bodary, S. In *Putting the Pieces Together: Contribution of Fluorescence Polarization Assays to Small-Molecule Lead Optimization*, Proceedings of SPIE: In-Vitro Diagnostic Instrumentation; Cohn, G. E., Ed.; SPIE: Washington, 2000; pp 128–137.